RAYMOND M. SOVA, MILTON J. LINEVSKY, MICHAEL E. THOMAS, and FRANK F. MARK

HIGH-TEMPERATURE OPTICAL PROPERTIES OF OXIDE CERAMICS

A vacuum emissometer utilizing a carbon dioxide laser for high-temperature sample heating has been designed and built at the Applied Physics Laboratory for use with a Fourier transform spectrometer. A two-color pyrometer technique is used to calculate sample temperature. Oxides such as sapphire, spinel, yttria, aluminum oxynitride, and fused silica are experimentally characterized at temperatures from 600 to 2000 K and at frequencies from 500 to 5000 cm^{-1}. A glowing yttria sample has also been characterized over the spectral range of 8500 to 13,500 cm^{-1}. Good agreement with a quantum mechanical multiphonon model for the complex index of refraction, also developed at APL, is obtained.

INTRODUCTION

Current characterization of optical materials is, in general, inadequate for many advanced applications. Manufacturers usually concentrate on material development instead. This inadequacy is especially true of the optical properties of infrared/radio frequency (IR/RF) dome materials being considered for use in missile guidance systems and thermally protective coatings for high-speed vehicles and combustors (e.g., the National Aerospace Plane).

Although we have witnessed many accomplishments in hypersonic IR guidance technology in the past few years, the critical issue of the high-temperature (>1000 K) extrinsic and intrinsic optical properties of candidate dome materials has not been fully addressed. This topic includes definitive measurements of IR emissivity and refractive index as a function of temperature. Infrared characterization of IR/RF dome materials is needed to support pyrometer design, which is used in high-temperature testing of radomes.

Past work at APL concerning the optical properties of materials has concentrated on transmittance and reflectance measurements as a function of frequency (100 to 20,000 cm^{-1}) and temperature (295 to 800 K), and development of semi-empirical theories that allow precise representation and meaningful interpolation and extrapolation of the experimental data.[1–9]

To continue the high-temperature experimental effort, we have constructed an emissometer utilizing a carbon dioxide laser and a Fourier transform spectrometer (FTS). The laser is used to heat only the sample to very high temperature so that no contaminating radiation from other hot surfaces degrades the emission spectrum. The FTS offers high throughput, high resolution, and, because of computer control, easy data manipulation. Emissometry is ideal for high-temperature optical property studies because sample emission is not a noise source as it is for transmission measurements; sensitive measurements are possible, and a direct measure of the absorption coefficient can be made when the emissivity is low.

The inclusion of multiphonon contributions is essential for modeling both the real and imaginary parts of the index of refraction. On the basis of past work concerning multiphonon sum band absorption theory and the Kramers–Krönig relation, the multiphonon contributions to the real part of the index of refraction are now included. Multiphonon refractive effects are important throughout the IR at high temperature and near the IR edge of transparency at room temperature.

We describe this recent experimental and theoretical progress in more detail in this article. The information was used to design two-color pyrometers for temperature measurements of oxide ceramics and to model emissivity in general. Good agreement is obtained between experimental emissivity and theory over the observed temperature range.

BACKGROUND

The optical properties of an insulating material can be specified completely by the complex index of refraction $\mathbf{n}(\nu, T)$ or complex permittivity $\epsilon(\nu, T)$, where ν is the spectral frequency in wave numbers (reciprocal wavelength) and T is temperature. The relationship between $\mathbf{n}$ and ϵ is

$$\mathbf{n}(\nu, T) = \sqrt{\epsilon(\nu, T)}\,, \tag{1}$$

where $\mathbf{n}(\nu) = n - jk$ (n is the index of refraction and k is the index of extinction). The absorption coefficient is defined by

$$\beta_a(\nu, T) = 4\pi k(\nu, T)\,. \tag{2}$$

In what follows, only intrinsic absorption losses will be considered.

The optical properties of a typical polar crystalline insulator are shown in Figure 1. In the IR, we see two main contributors to the complex index of refraction of insulating ceramics: electronic transitions (areas shaded

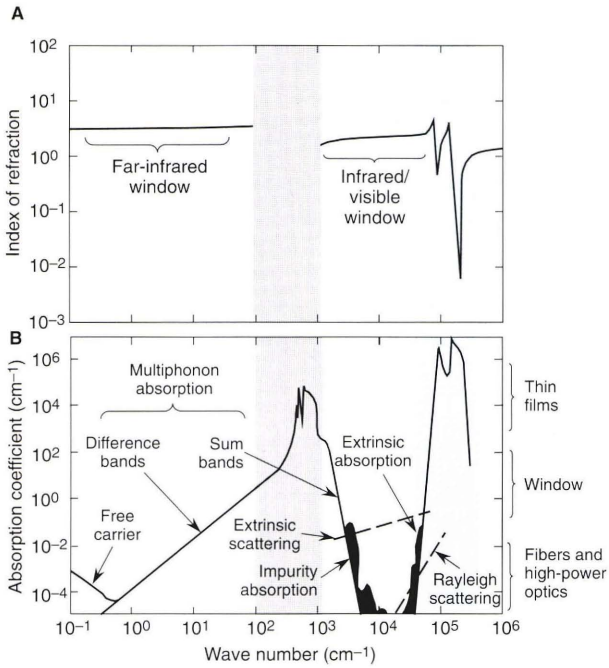

Figure 1. Optical properties of a typical polar crystalline insulator. **A.** Index of refraction. **B.** Absorption coefficient. Areas shaded blue represent lattice vibrations; those shaded gray represent electronic band transitions.

gray) and lattice vibrations (shaded blue) or phonons (a vibrational wave packet). The electronic transitions contribute to the real part of the index of refraction only in the form of a frequency-independent parameter with weak temperature dependence. Most of the frequency and temperature dependence of the complex index of refraction at mid-IR frequencies comes from phonons. Thus, the discussion will concentrate on one-phonon and multiphonon contributions.

One-Phonon Bands

One-phonon absorption processes are due to the excitation of a phonon upon the absorption of a photon. These processes are very strong, since the photons couple directly to the fundamental lattice vibrations of a material. The classical pole-fit model[1] has been used to model the one-phonon absorption processes. Each vibrational mode of a material is modeled as a mathematical pole (i.e., the magnitude of the function goes to infinity at the position of the pole). Each mode has a specified strength and width. This model represents ϵ in terms of the lattice vibrations:

$$\epsilon(\nu,T)=\epsilon_\infty(T)-\sum_i \frac{\Delta\epsilon_i(T)\nu_i^2(T)}{\nu_i^2(T)-\nu^2+j\gamma_i(\nu,T)\nu}, \qquad (3)$$

where $\Delta\epsilon_i$, γ_i, and ν_i are the ith mode strength, line width, and long-wavelength transverse optical frequency, respectively. The sum on "i" is over all transverse optical modes, and ϵ_∞ is the permittivity measured at optical frequencies. This model is known to describe **n** adequately in the IR/RF regions.[1,2] The temperature dependence of ϵ_∞, $\Delta\epsilon_i$, and ν_i is assumed linear, and that of γ_i is assumed quadratic. The implied frequency dependence of γ_i represents a cutoff beyond the one-phonon region caused by anharmonicities of the potential.

The magnitude of the single-surface reflectance $|R|$ of a medium (at normal incidence) is

$$|R|=\frac{(n-1)^2+k^2}{(n+1)^2+k^2}. \qquad (4)$$

In general, a measurement of $|R|$ is not sufficient to determine ϵ (e.g., both n and k). The classical pole-fit model, however, satisfies the Kramers-Krönig relation and therefore provides a relationship between n and k that allows one to construct a physically meaningful representation of ϵ using only the magnitude of R as input.

Multiphonon Sum Bands

Multiphonon absorption processes are due to the excitation of more than one phonon upon absorption of a photon. These processes become important in the transparent regions of a material where one-phonon absorption processes do not dominate. Difference bands of multiphonon absorption occur in the millimeter spectral region, and sum bands occur in the IR region. Sum band processes dominate IR emissivity.

Previously, a multiphonon absorption model was developed at APL to characterize absorption coefficient contributions from multiphonon sum band processes.[3,4] The model is based on the Morse interatomic potential, given by

$$V(r)=D\left\{1-\exp\left[-a(r-r_0)\right]\right\}^2, \qquad (5)$$

where

$V(r)$ is the energy potential for a material,
r is the distance from the center of the molecular system,
D is the dissociation energy,
a is a function of the fundamental lattice-vibration frequency and reduced mass, and
r_0 is the location of the equilibrium position.

This potential leads to an exact solution to the Schrödinger equation with anharmonicity. Three parameters of a given material are required as inputs to the multiphonon model: (1) a scaling constant K, (2) the dissociation energy D, and (3) the maximum longitudinal optical mode frequency $\nu_{max.}$ All of these parameters can be obtained from room temperature absorption data (see Ref. 3 for more details).

The model has recently been extended to include multiphonon contributions to the real part of the index of refraction.[5] Although multiphonon contributions are typically very small at room temperature (295 K), the magnitudes of the higher-order modes increase significantly with temperature. Above the Debye temperature, the temperature dependence of the ith mode is about T^{i-1} (Ref. 3).

The multiphonon sum band contributions to the absorption coefficient β_i and the index of refraction n_i for

sapphire ordinary ray (o-ray) at 295 K are shown in Figure 2. The spectral shape of β_i for the ith phonon mode is Gaussian, and the spectral shape of the sum of β_i for i = 2, 3, 4, 5, and 6 is exponential. The spectral shape of n_i for the ith phonon mode has a typical anomalous dispersion character. The magnitudes of n_i for higher-order modes are very small at 295 K but become larger with increasing temperature. For clarity, the plots of n_i for higher-order modes (i = 3, 4, and 5) are normalized with respect to the second-order mode. The scaling factors are given in Figure 2B as are the zero crossover frequencies that correspond to $n_i = 0$.

Emissivity Model

Materials heated to high temperatures (≈2000 K) strongly emit IR radiation. (The peak emission of a 2000 K blackbody is located at a wavelength of 2.6 μm.) The radiance of a material, $L_M(\nu, T)$, is defined as the flux per unit projected area per unit solid angle [W/(m^2 – sr)], and is expressed as

$$L_M(\nu, T) = \epsilon_v(\theta, T) L_{BB}(\nu, T), \qquad (6)$$

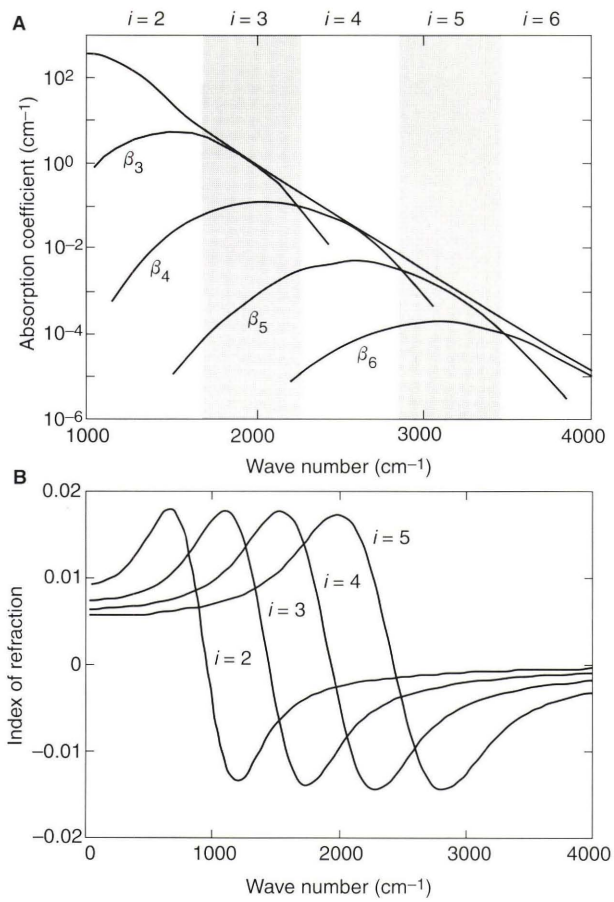

Figure 2. Multiphonon sum band contributions of sapphire ordinary ray at 295 K: **A.** To the absorption coefficient β_i for i = 2 to 6; **B.** To the index of refraction n_i for i = 2 to 5. Scaling factors and zero crossover frequencies (cm^{-1}) for n_i are, respectively, 1 and 958 for i = 2; 9 and 1450 for i = 3; 5000 and 1940 for i = 4; and 1.7 × 10^5 and 2430 for i = 5.

where $\epsilon_v(\theta, T)$ is the spectral emissivity of the material, $L_{BB}(\nu, T)$ is the radiance of a blackbody, and θ is the angle of incidence (i.e., the angle between the surface normal and the incident ray). In general, the emissivity is composed of two components: specular and diffuse. For our samples, the diffuse component is negligible, since the samples have smooth, flat surfaces and negligible bulk scattering.

On the basis of the total power law and Kirchhoff's law of radiation, the specular component of emissivity can be expressed as

$$\epsilon_v(\theta, T) = \frac{(1-R)\left[1-\exp\left(-\beta_a l/\cos\theta\right)\right]}{1-R\exp\left(-\beta_a l/\cos\theta\right)}, \qquad (7)$$

where l is the sample thickness. In general, ϵ_v and R depend on the angle of incidence, but for near-normal incidence, these dependencies can be neglected. This approximation is valid for our experiment, since the collecting optics limit the field of view of the sample to less than 7° from normal. Theoretical emissivity curves are generated by using Equations 2, 4, and 7 along with n and k values calculated with the one-phonon and multiphonon models. A comparison between theoretical emissivity and the experimental data will be described later.

EXPERIMENT

A photograph of the experimental setup is shown in Figure 3. The helium neon (HeNe) laser beam indicates the optical path taken by the CO_2 laser. (A turbomolecular pump used to evacuate the sample chamber is not shown.) A schematic of the experimental setup is presented in Figure 4. The major components are a 50-W CO_2 laser, high-vacuum emissometer chamber, 1273 K blackbody, and the FTS. In this experiment, a sample is heated to high temperatures using the CO_2 laser. The IR radiation emitted by the sample is measured with the spectrometer. The experiment is calibrated by measuring the IR radiation emitted by the blackbody. Details of the experimental components and measurement procedure follow.

Experimental Components

A 50-W CO_2 laser tuned to the 9- or 10-μm spectral region was chosen to heat the samples, since all of the oxide materials being studied (sapphire, yttria, aluminum oxynitride [ALON], spinel, and fused silica) strongly absorb radiation in these regions. For example, a 0.1-cm-thick sapphire sample absorbs ≈95% of the incident laser energy at 9.6 μm. The samples are heated uniformly by using the TEM_{00} laser mode. To reduce thermal shocking of the samples, an optical attenuator is used while controlling the laser current to slowly increase the amount of laser power incident on the samples.

Depending on the spectral range of the measurement, barium fluoride (BaF_2) or zinc selenide (ZnSe) lenses are used to collimate the radiation emitted from the emissometer chamber and the 1273 K blackbody reference. The position of the mirror inside the optical junction box shown in Figure 4 is used to select between the collimated radi-

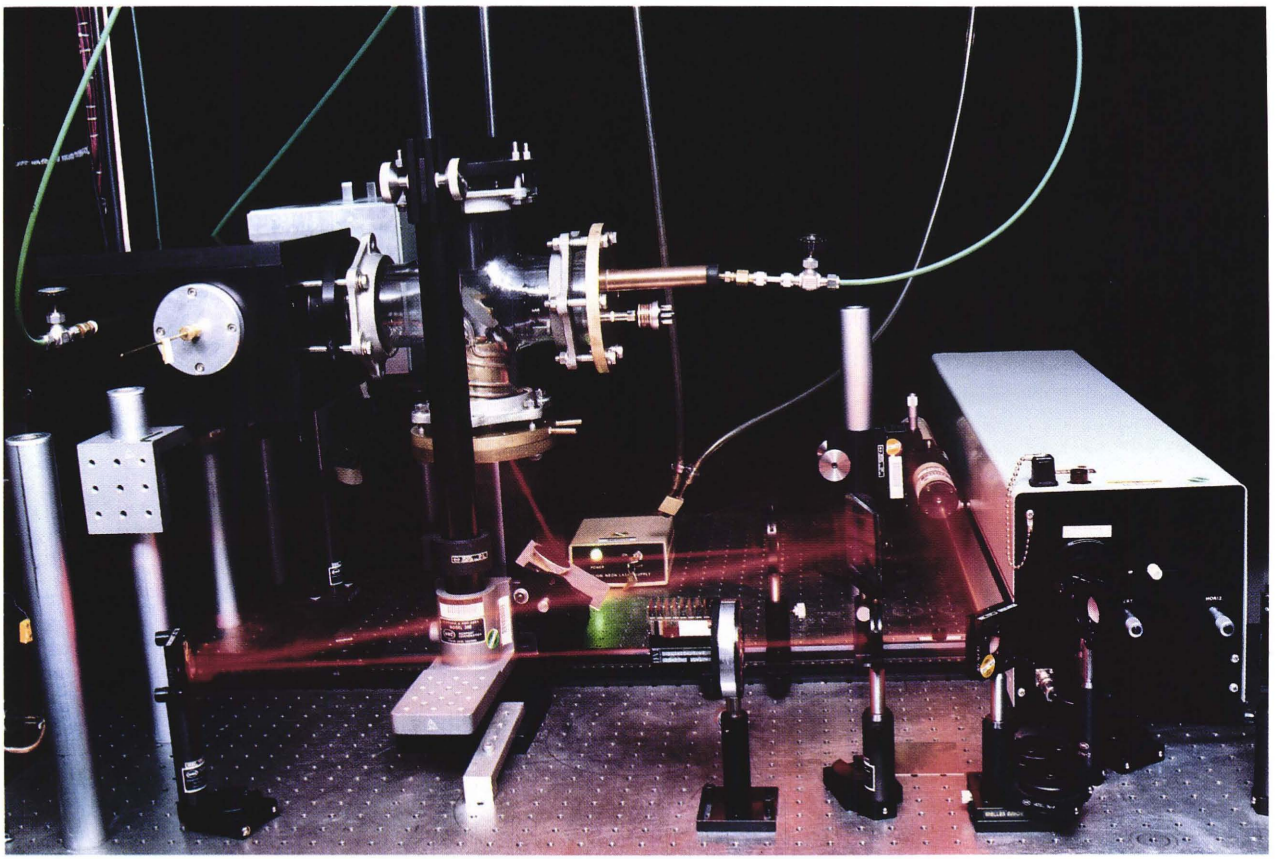

Figure 3. Photograph of laser emissometer experiment. The HeNe laser beam traces the optical path of the CO_2 laser beam.

ation emitted from either the 1273 K blackbody or the sample chamber. A BaF_2 (or ZnSe) lens in the optical junction box is used to couple the radiation optimally to the spectrometer. The junction box and spectrometer are evacuated to pressures below 5 Torr to eliminate spectral contamination from atmospheric CO_2 and H_2O. A potassium bromide beam splitter and a mercury–cadmium–telluride detector are used in the spectrometer to make measurements over the spectral range of 500 to 5000 cm^{-1}.

The 1273 K blackbody is used to obtain the instrument response function for the experimental setup. This function allows one to factor out the spectral characteristics of all optical components between the sample and detector and also the spectral response of the detector. The optical path of the blackbody is closely matched to that of the emissometer chamber (i.e., all lenses, windows, etc., used in the two paths are identical). Since the blackbody cannot be evacuated, a nitrogen purge is used to minimize CO_2 and H_2O contamination. The resulting intensities are relative, however, because the radiation areas of the blackbody and sample cannot be made identical.

The emissometer chamber consists of a sample holder mounted into the bottom of a Pyrex cross. All four ends of the cross are vacuum sealed so the chamber can be evacuated independent of the rest of the system. A turbomolecular pump is attached to one end of the chamber to achieve vacuum levels of $\approx 10^{-7}$ Torr. These vacuum levels are desired to minimize heat loss from the sample through gas convection and conduction.

A photograph and diagram of our current sample holder are shown in Figures 5 and 6, respectively. Four tubular alumina legs are cemented to an anodized aluminum base using a low-vapor-pressure epoxy. Type-S thermocouples are attached to each leg just below the irradiated face of a sample. These serve to detect beam misalignment and misfocusing and to verify uniform irradiation. A sample is placed on the tips of four platinum wires attached to the tops of the alumina posts. The small contact area of the wire tips minimizes heat loss via conduction from the hot sample to the cool alumina posts. The wires are placed near the edges of the sample to minimize background radiation emitted from the hot wires. Platinum is used because of its high-melting-point temperature (2045 K) and inertness.

A ZnSe negative lens mounted in the bottom flange of the sample holder expands the CO_2 laser beam to a size that evenly illuminates the entire lower face of a sample (Fig. 6). The lens is antireflection-coated to achieve $\approx$99% transmittance at laser wavelengths near 10.6 μm. The lens is positioned such that the laser beam hits the sample at an off axis angle (15°) to minimize the amount of laser radiation that can enter the spectrometer—especially in the event of sample breakage.

A water-cooled cylindrical brass top hat is mounted over the sample holder to minimize background radiation

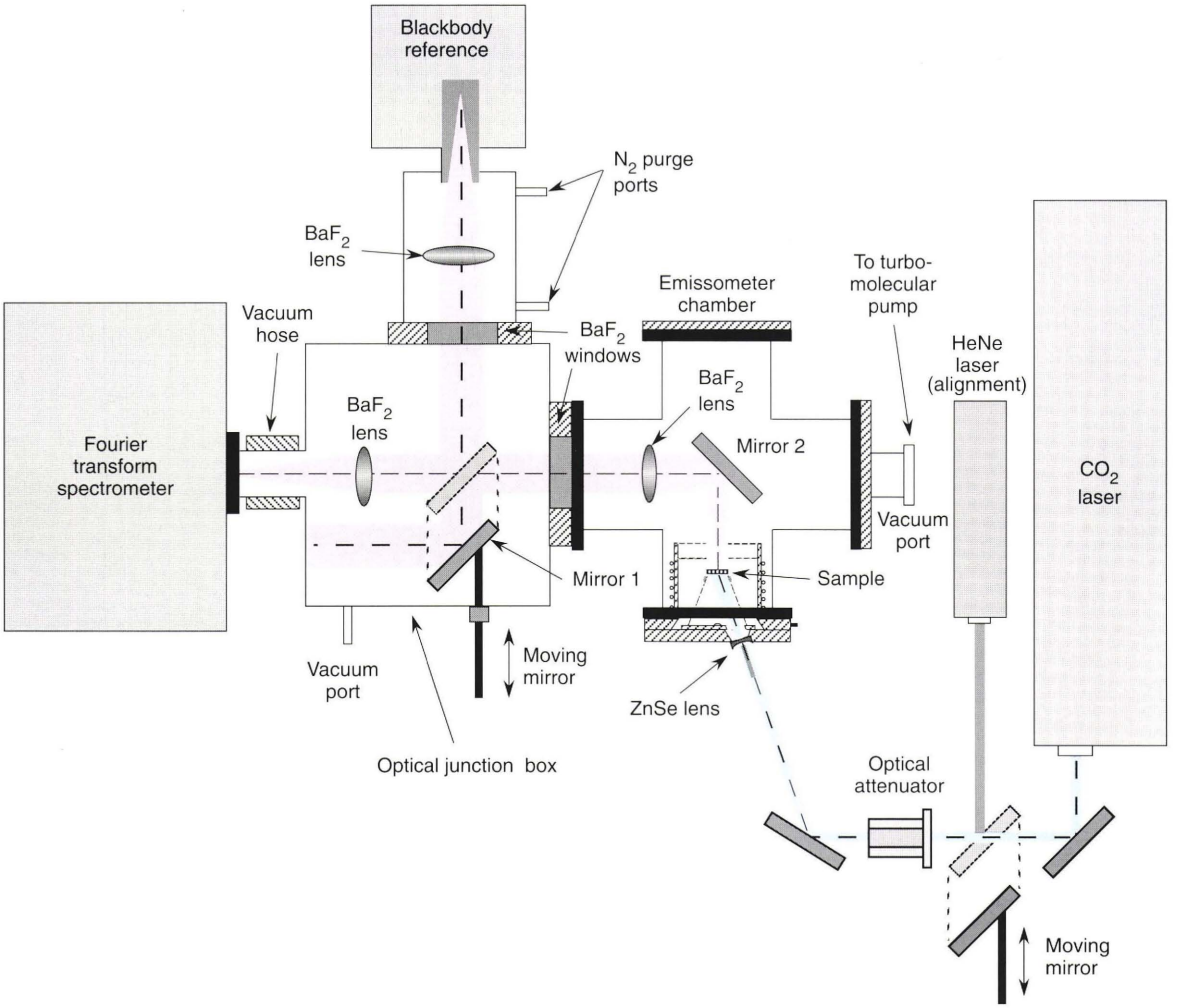

Figure 4. Diagram of experimental setup showing the CO_2 laser, blackbody, emissometer chamber, and spectrometer.

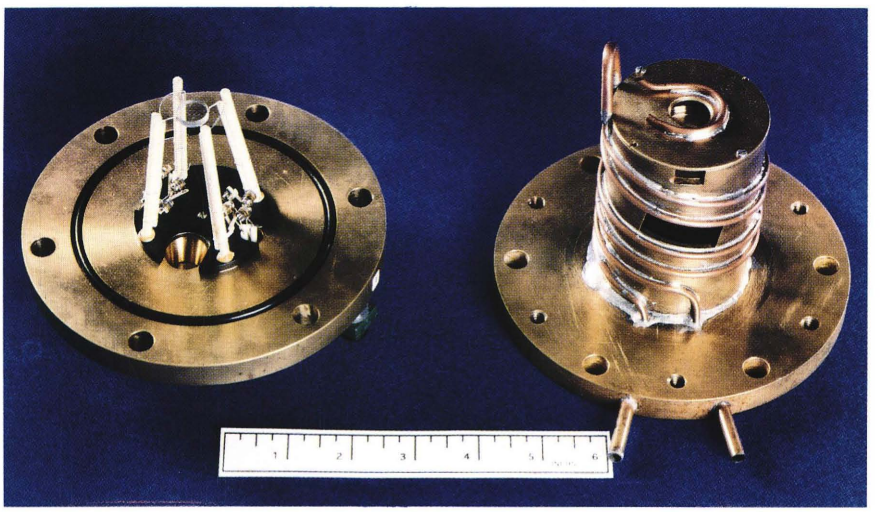

Figure 5. Photograph of the emissometer chamber comprising a sample holder and a water-cooled cylindrical brass top hat. A 12.7-mm-dia. fused silica sample is shown mounted in the sample holder.

and also to protect the Pyrex cross from the CO_2 laser beam. A series of circular apertures are mounted inside the top hat above the sample to confine the field of view of the spectrometer to the central area (≈3-mm-dia.) of the sample and minimize stray background radiation (especially stray radiation from the CO_2 laser). It is important to look only at a small area at the center of the sample since the laser heating is nonuniform and a

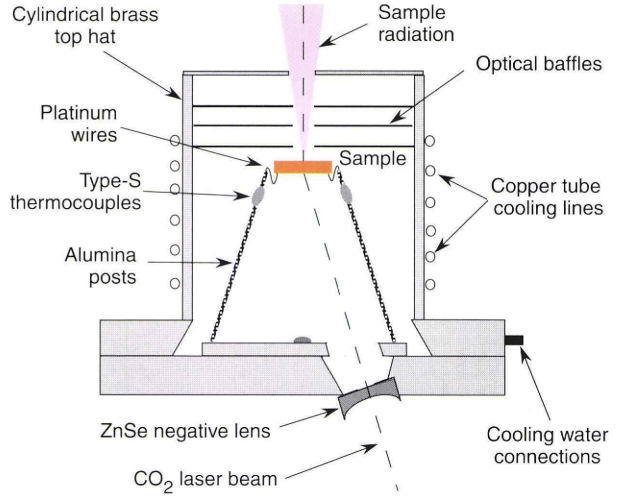

Figure 6. Diagram of emissometer sample chamber showing the sample location, CO_2 laser beam, optical baffles, and cooling lines.

temperature gradient develops between the center and edges of the sample.

Measurement Procedure

After the emissometer and blackbody are aligned to the FTS and the CO_2 laser beam is aligned to the sample, a room temperature background spectrum is measured by looking at the central area of an unheated sample. (We have observed that most background radiation comes from inside the spectrometer.) Next, a spectrum of the 1273 K blackbody is measured. Finally, the sample is slowly heated with the CO_2 laser, and a series of spectra are measured at different points during the heating process. Each measurement is taken after the sample has achieved steady state.

Sample Temperature Determination

We need to know accurately the temperature of the sample to determine its emissivity, since, by definition, the emissivity is the ratio of the emittance of the sample to the emittance of a blackbody at the same temperature and frequency. For the materials investigated in this program, we used a two-color pyrometer technique for temperature determination, since all these material have spectral regions in which their emissivities are well-known and close to unity.[2] These spectral regions, although somewhat limited in frequency, occur in the two-phonon region, which lies to the red of the multiphonon absorption edge and to the blue of the one-phonon bands of these materials.

In the two-color pyrometer technique, the ratio of intensities at two different frequencies is measured, and if the emissivities are known at the two frequencies, the ratio is a unique function of temperature expressed as

$$R_{12}(T) = \frac{\epsilon_1 L_{BB}(\nu_1, T)}{\epsilon_2 L_{BB}(\nu_2, T)}, \qquad (8)$$

where R_{12} is the ratio of intensities at frequencies ν_1 and ν_2, ϵ_1 and ϵ_2 are the spectral emissivities at frequencies ν_1 and ν_2, and $L_{BB}(\nu_1, T)$ and $L_{BB}(\nu_2, T)$ are the blackbody functions at frequencies ν_1 and ν_2, respectively, and at temperature T.

In practice, the frequencies ν_1 and ν_2 are chosen to cover the largest spread possible for which the corresponding emissivities are known. The ratio in Equation 8 is plotted as a function of T for each material. Since this ratio is monotonic in temperature, the sample temperature can be uniquely determined from a given measured intensity ratio. A typical plot for sapphire of R_{12} versus T is shown in Figure 7. The sensitivity of this technique diminishes with increasing temperature as shown in the figure. Near 2000 K, a small change in the ratio R_{12} can field a large change in the predicted temperature.

Another method to calculate sample temperature is used in conjunction with the two-color technique at high temperatures. The multiphonon absorption edge shifts to higher frequencies with increasing temperature. The multiphonon model predicts this shift well. By fitting the model to the experimental data, the sample temperature can be calculated. Using both the two-color technique and the multiphonon edge technique, the sample temperature can be calculated more accurately at high temperatures.

Calculating Sample Emissivity

The following analytical procedure is used to calculate the sample emissivity from the measured spectra.

1. Subtract room temperature background spectrum from the 1273 K blackbody spectrum and raw sample spectrum.
2. Calculate the instrument response function by dividing the experimental 1273 K blackbody spectrum by a theoretical 1273 K blackbody spectrum.
3. Calculate the sample emission spectrum by dividing the raw sample spectrum by the instrument response function.
4. Calculate the sample temperature using the two-color pyrometer technique.
5. Calculate the emissivity of the sample by dividing the sample emission spectrum by a theoretical blackbody spectrum at the calculated sample temperature.

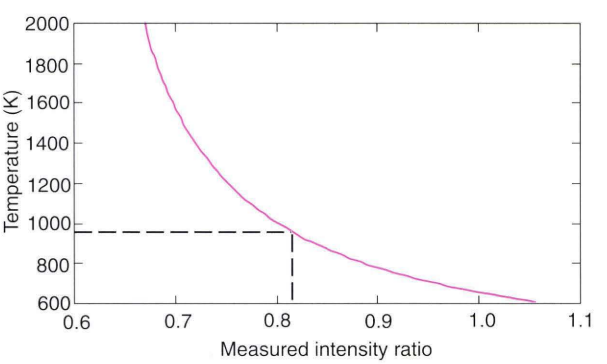

Figure 7. Two-color pyrometer curve for sapphire. The intensity ratio of 0.816 corresponds to a temperature of 950 K. Frequencies ν_1 and ν_2 = 1050 and 1400 cm^{-1}, respectively. Spectral emissivity ratio $(\epsilon_1/\epsilon_2) = 1.03$.

6. Normalize the emissivity spectrum by setting the emissivity value near 10 μm to the value predicted by the model. Typically, this value is ≈0.995 and does not change with temperature.

RESULTS

Preliminary emissometer measurements were performed with 25.4-mm-dia. samples mounted in a nitrogen-purged sample chamber. Heat losses by gas convection and conduction made it difficult to heat the samples without causing them to break. The maximum temperature achieved with this setup was 1100 K. The emissivity of an IR-grade sapphire o-ray sample obtained in these preliminary experiments is shown in Figure 8. The absorption feature seen at 1600 cm^{-1} is due to background H_2O. The amount of background H_2O spectra is low enough to measure the sample temperature reliably with the two-color technique. The temperature was found to be 975 K, ±50 K. Of particular note is the observation of the broad OH impurity emission that covers a spectral region from 2600 to 3500 cm^{-1}. The spectral feature at about 1240 cm^{-1} was later found to be due to contamination of one of the mirrors in the setup.

Our ability to heat samples to higher temperatures was dramatically improved by using 12.7-mm-dia. samples mounted in the high-vacuum sample chamber previously described. The samples were less prone to breakage, although some did develop hairline cracks at high temperatures. Unlike any of the samples heated in a nitrogen purge, all samples heated in vacuum began to glow at temperatures above 1000 K. Temperatures near 2000 K were achieved with sapphire, yttria, and spinel. Figure 9 shows a glowing sapphire sample whose temperature is near 1900 K. We next describe in detail sapphire data and present the highest temperature emissivity data for yttria, spinel, fused silica, and ALON.

A family of emission curves for a UV-grade sapphire o-ray sample (12.7-mm-dia., 1.0-mm-thick) is shown in Figure 10. As the sample is heated, the emission intensity increases, and the peak of the emission spectrum shifts to higher frequencies, as expected. These curves are obtained by following the first three steps in the analytical procedure described previously. The sample temperature is found from these curves using the two-color pyrometer technique.

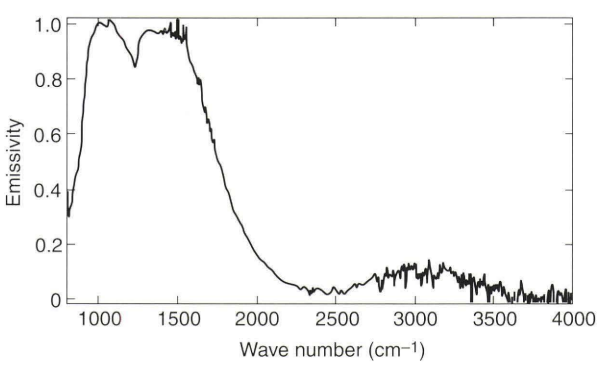

Figure 8. High-temperature (975 K) spectral emissivity of an IR-grade sapphire ordinary ray sample (25.4-mm-dia., 1.0-mm-thick).

To illustrate the two-color technique, the temperature for the emission curve for sapphire corresponding to the data file is calculated. We have observed that ϵ_1 and ϵ_2 are approximately independent of temperature when ν_1 and ν_2 are chosen in the two-phonon region. The frequencies ν_1 = 1050 cm^{-1} and ν_2 = 1400 cm^{-1} and emissivities $\epsilon_1 = 0.995$ and $\epsilon_2 = 0.967$ were obtained from a theoretical emissivity plot of sapphire. The emissivity values are fairly accurate, since the model has been validated experimentally to temperatures of 800 K. The intensity ratio $I(\nu_1)/I(\nu_2) = 0.816$ is obtained from the emission curve for the data file shown in Figure 10. This ratio corresponds to a temperature of 950 K as indicated by the two-color pyrometer curve shown in Figure 7. Each emission curve is analyzed in this manner.

The resulting emissivity plots for the UV-grade sapphire o-ray sample are shown in Figure 11. The temperature range is from 950 to 1930 K, ±50 K. As temperature increases, the edge near the one-phonon region (≈900 cm^{-1}) shifts downward in frequency, and the multiphonon absorption edge (≈1800 cm^{-1}) shifts upward in frequency. The spectral feature at 1050 cm^{-1} (seen more clearly in Fig. 12B) is due to stray radiation from the CO_2 laser, and the feature at 1240 cm^{-1} is a remnant of the mirror contamination. Even at high temperatures, the UV-grade sapphire o-ray has negligible emission above the multiphonon absorption edge (≈1800 cm^{-1}). In comparison, the lower-quality IR-grade sapphire o-ray sample has strong OH impurity emission at 3100 cm^{-1} (see Fig. 7).

Figures 12A and 12B compare the experimental and theoretical emissivity data for UV-grade sapphire o-ray at 750 and 1930 K, ±50 K, respectively. At 750 K, the theoretical data agree very well with the experimental data as expected, since both the one-phonon and multiphonon models have been validated by reflectance and transmittance measurements for temperatures as high as 800 K. At 1930 K, the multiphonon model is in very good agreement with experimental data in the two-, three-, and four-phonon regions (≈900 to ≈2700 cm^{-1}), whereas the one-phonon model does poorly at fitting the experimental data at the edge of the one-phonon region (≈900 cm^{-1}). The current one-phonon model was not expected to work above 1000 K since it does not incorporate cross-coupling of vibrational modes that can become important at high temperatures. Free carrier effects may also become important at high temperatures.

The high-temperature IR and near-IR/visible emissivity spectra of yttria are shown in Figure 13. The yttria sample was glowing white hot at 2000 K, ±50 K. Unlike sapphire, the IR emissivity of yttria becomes significant at high temperatures in the transparent region above the multiphonon edge (>1100 cm^{-1}). The preliminary near-IR/visible (8500 to 13,500 cm^{-1}) measurements indicate that the emissivity continues to increase throughout the visible region. Brecher et al.[10] observed similar results for lanthana-strengthened yttria and noted a significant increase in emissivity above 1200 K. They attributed the increase to oxygen point defects (oxygen interstitials and

Figure 9. Photograph of a glowing sapphire sample at 1900 K.

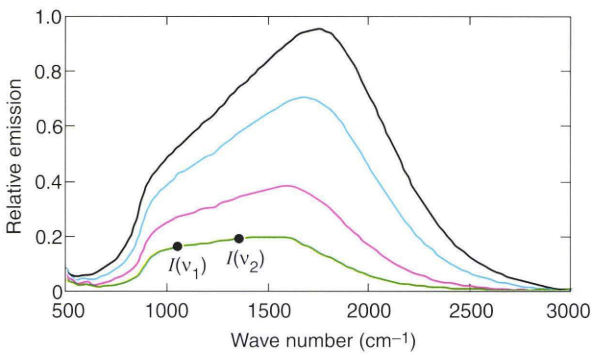

Figure 10. High-temperature spectral emission of a UV-grade sapphire ordinary ray sample (12.7-mm-dia., 1.0-mm-thick) at 950 K (green curve), 1230 K (red), 1630 K (blue), and 1930 K (black). $I(\nu_1)$ and $I(\nu_2)$ are the intensity positions chosen for the two-color technique.

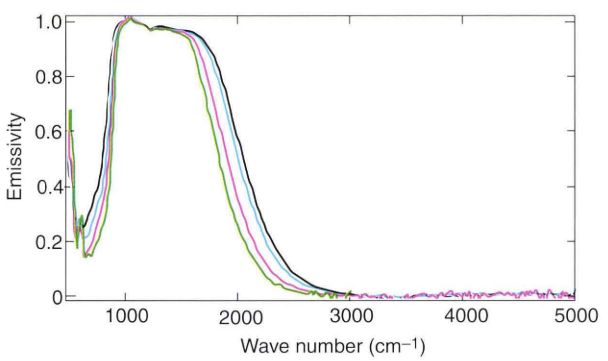

Figure 11. High-temperature spectral emissivity of a UV-grade sapphire ordinary ray sample (12.7-mm-dia., 1.0-mm-thick) at temperatures noted in Figure 10.

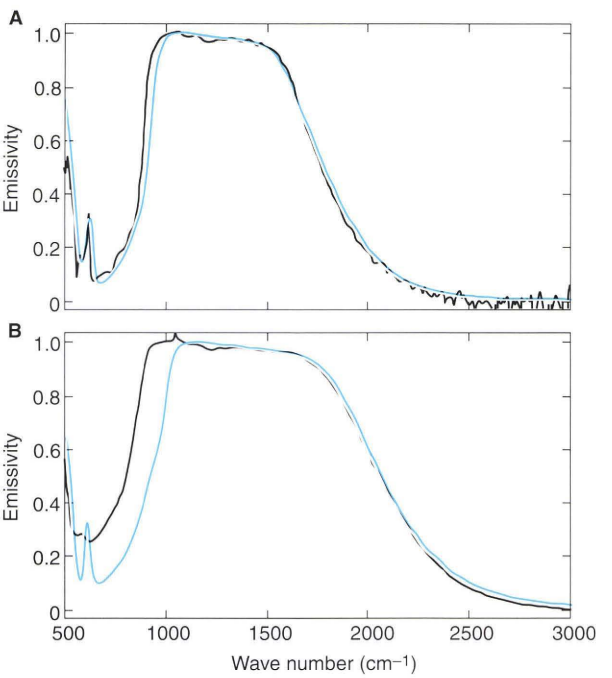

Figure 12. Comparison between experimental (black curves) and theoretical (blue curves) emissivity of a UV-grade sapphire ordinary ray sample (12.7-mm-dia., 1.0-mm-thick). **A.** 750 K. **B.** 1930 K.

vacancies). These defects alter the bandgap of a material and allow free carriers to be thermally liberated. The vacuum environment enhances the occurrence of such defects.

In addition to the experimental emissivity curves for yttria, Figure 13 also includes a theoretical emissivity

curve based on the one-phonon and multiphonon models. Again, the one-phonon model breaks down at the emissivity edge in the one-phonon region. The multiphonon model is in good agreement with the data in the two-phonon region and at the multiphonon absorption edge. As expected, the multiphonon model does not predict the increase in emissivity above the multiphonon absorption edge.

The high-temperature IR emissivity of spinel is shown in Figure 14. The spinel sample was glowing white hot at 2000 K, ±50 K. Again, the one-phonon model fits poorly near the emissivity edge in the one-phonon region, and the multiphonon model fits very well in the two- and three-phonon regions. Also, remnants of the mirror contamination can be seen at 1240 cm^{-1}. The emissivity is very low in the region above the multiphonon edge (>3000 cm^{-1}).

The high-temperature IR emissivity of fused silica is shown in Figure 15. The fused silica sample could only be heated to ≈1300 K, ±100 K, since the absorption at the laser wavelength of 10.28 μm is only ≈90.0%, and the radiative losses are increased because the fused silica samples (3.175-mm) are over three times thicker than the rest of the samples (1.0-mm). The spectral features centered at 3600 cm^{-1} and 4500 cm^{-1} are due to OH and/or H_2O impurities commonly found in fused silica. Since fused silica is an amorphous material with very broad vibrational modes that are spread far apart in frequency, its optical properties are difficult to model with the one-phonon and multiphonon models. These models are ideally suited for crystalline materials that have sharp vibrational modes. The best attempt to fit the model to the experimental data is shown in Figure 15. The temperature is known less accurately for fused silica (±100 K).

An earlier measurement of the high-temperature spectral emissivity for an ALON sample taken in the nitrogen-purged sample chamber is shown in Figure 16. The spectral features caused by the mirror contamination centered at 1240 cm^{-1} and background H_2O centered at 1700 cm^{-1} are clearly seen. The calculated temperature is 960 K, ±50 K. The one-phonon model fits the data very well. As observed in previous transmittance data,[3] the multiphonon model poorly fits the experimental data in the two-phonon region. This discrepancy may be due to the crystal structure of ALON, which produces many broad, closely spaced vibrational modes. The two-phonon density of states for ALON is non-Gaussian, which is in disagreement with the Gaussian assumption used in the multiphonon model.

Two attempts were made to heat ALON samples (12.7-mm-dia., 1.0-mm-thick) in the vacuum emissometer at temperatures above 1000 K. During both attempts, the samples would heat up to a glowing orange and emit the same amount of radiation as indicated by the central burst

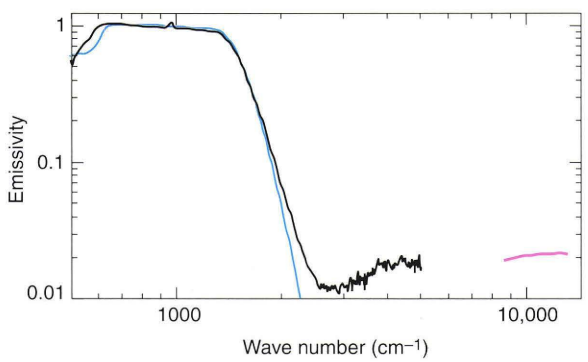

Figure 13. High-temperature spectral emissivity of a yttria sample (12.7-mm-dia., 1.0-mm-thick) at 1950 K (black curve) in the IR (500 to 5000 cm^{-1}) and ≈1900 K (red curve) in the near-IR and visible (8500 to 13,500 cm^{-1}). A theoretical plot of emissivity (blue curve) for the infrared region is also shown.

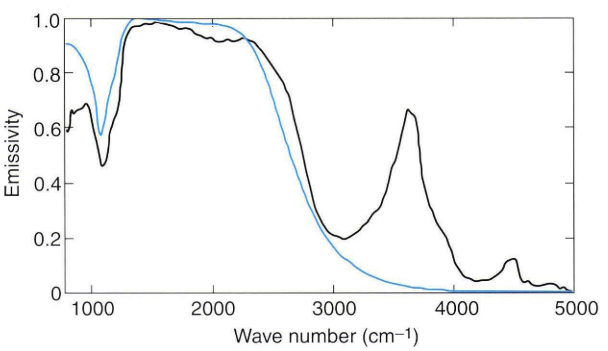

Figure 15. High-temperature spectral emissivity of a fused silica sample (12.7-mm-dia., 3.175-mm-thick) at 1300 K (experimental, black curve; theoretical, blue curve).

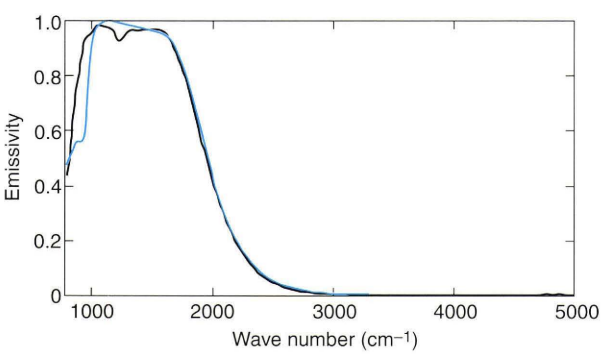

Figure 14. High-temperature spectral emissivity of a spinel sample (12.7-mm-dia., 1.0-mm-thick) at 2000 K (experimental, black curve; theoretical, blue curve).

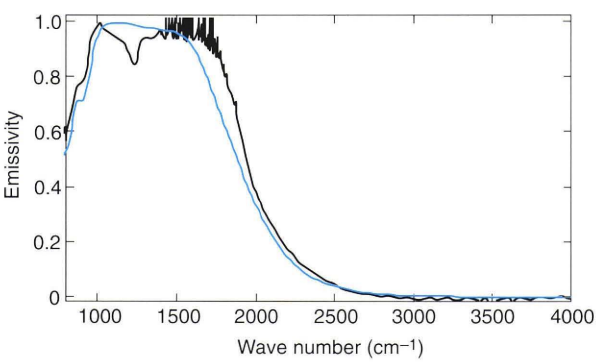

Figure 16. High-temperature spectral emissivity of an ALON sample (12.7-mm-dia., 1.0-mm-thick) at 960 K (experimental, black curve; theoretical, blue curve).

signal on the FTS. At that point, any increase in laser fluence on the sample would not increase the emission signal (i.e., central burst signal on the FTS). Increasing the laser fluence further caused both samples to break. The properties of the material seemed to change at this temperature. Possibly a phase transformation was occurring and/or the reflectance at the laser wavelength was increasing. Unfortunately, the data for these runs seemed to be corrupted and could not be analyzed. Further studies are needed.

CONCLUSIONS

A vacuum emissometer has been built at APL to study the high-temperature optical properties of oxide materials. The IR emissivity values of crystalline sapphire, spinel, yttria, ALON, and fused silica were measured from 600 to 2000 K over the spectral range of 500 to 5000 cm^{-1}. The region of high emissivity in these samples was used to determine the surface temperature by a two-color pyrometer technique.

The theoretical emissivity curves calculated with our previously developed multiphonon model compare favorably with experimental results over the entire temperature range in the multiphonon region. At high temperatures (>1000 K), the one-phonon model poorly reflects the emissivity edge near the one-phonon region (≈900 cm^{-1}), as expected. Effects due to cross-coupling between the vibrational modes are not included in the one-phonon model and may become important, along with free carrier absorption, at high temperatures.

Our results indicate that other absorption mechanisms become important at high temperatures. For example, OH impurities cause strong emission near 3100 cm^{-1}, and oxygen point defects may have caused the increase in emissivity observed for yttria in the spectral region of transparency between the multiphonon absorption edge and UV absorption edge. Future work will consider these absorption mechanisms along with another one-phonon model incorporating cross-coupling of vibrational modes.

The apparent increase in emissivity with temperature in the near-IR and visible regions is particularly interesting since this result is not predicted by any current model and may be very important in advanced sensor applications utilizing the visible region. The extension of these emissivity measurements, especially at high temperatures, into the visible and near-UV regions is necessary to extend the modeling effort into these regions by providing a database for comparison.

ACKNOWLEDGMENTS: This work was supported by Independent Research and Development funds at APL in the Optical Technology Program under the direction of William J. Tropf and in the Advanced Materials Technology Program under the direction of Lawrence W. Hunter. The authors wish to thank James Clinedinst and Craig Rice for their technical expertise in the development and construction of the emissometer chamber.

REFERENCES

[1] Hoffmann, C. E., "Optical Constants of Infrared Active Phonons as a Function of Frequency and Temperature," Master of Science Thesis, The Johns Hopkins University, Baltimore, Md. (1988).

[2] Hoffmann, C. E., Thomas, M. E., and Joseph, R. I., "The Infrared Emission Properties of Polar Crystals," in *Proc. 10th Symp. of Thermophysical Properties*, National Bureau of Standards, Gaithersburg, Md., p. 107 (Jun 1988).

[3] Thomas, M. E., Joseph, R. I., and Tropf, W. J., "Infrared Transmission Properties of Sapphire, Spinel, Yttria, and ALON as a Function of Temperature and Frequency," *Appl. Opt.* **27**, 239–245 (1988).

[4] Thomas, M. E., and Joseph, R. I., "A Comprehensive Model for the Intrinsic Transmission Properties of Optical Windows," *Proc. SPIE* **929**, 87–93 (1988).

[5] Sova, R. M., and Joseph, R. I., *Implementation of the Multiphonon Real Index of Refraction Model*, JHU/APL F1F(1)91-U-142 (1991).

[6] Joseph, R. I., and Thomas, M. E., "Differential Reflection Spectroscopy: A Direct Determination of Long Wavelength Optical Mode Frequencies in Polar Crystals," *Phys. Stat. Sol. (B)* **141**, K163–166 (1987).

[7] Thomas, M. E., and Joseph, R. I., "The Infrared Properties of Polar Crystals," *Johns Hopkins APL Tech. Dig.* **9**, 328–338 (1988).

[8] Thomas, M. E., "The Infrared Properties of the Extraordinary Ray Multiphonon Processes of Sapphire," *Appl. Opt.* **28**, 3277–3278 (1989).

[9] Thomas, M. E., "A Computer Code for Modeling Optical Properties of Window Materials," *Proc. SPIE–Window and Dome Technologies and Materials* **1112**, 260–267 (1989).

[10] Brecher, C., Wei, G. C., and, Rhodes, W. H., "Point Defects in Optical Ceramics: High-Temperature Absorption Processes in Lathana-Strengthened Yttria," *J. Am. Ceram. Soc.* **73**, 1473–1488 (1990).

THE AUTHORS

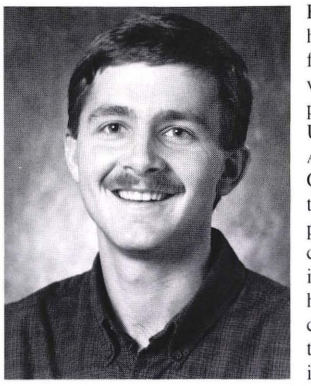

RAYMOND M. SOVA received his B.S. in electrical engineering from the Pennsylvania State University and his M.S. in applied physics from The Johns Hopkins University. He is a member of APL's Electro-optical Systems Group, where he has worked on the development of a digital signal processing algorithm for electronically scaling and rotating digital images and the development of high-temperature (>77 K) superconducting thin-film radiation detectors. Current research interests include the development of a laser remote sensing system for measuring atmospheric humidity and temperature profiles and spectroscopic studies of oxide materials and atmospheric gases.

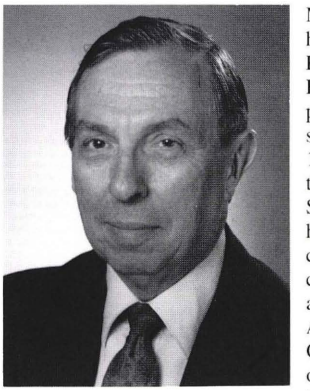

MILTON J. LINEVSKY received his B.S. in chemistry from the Rensselaer Polytechnic Institute. He received his M.S. and Ph.D. in physical chemistry from the Pennsylvania State University. From 1957 to 1979, he was a member of the General Electric Company's Space Sciences Laboratory, where he conducted research on spectroscopy of high-temperature species, chemical kinetics, and chemical and metal vapor lasers. He joined APL in 1979 as part of the Research Center and is presently a member of the Aeronautics Department. His research interests include combustion and flame chemistry, spectroscopic and radiometric properties of materials, high-speed flow diagnostics, and beam surface interactions. He is a member of the Vehicle Interactions Program team.

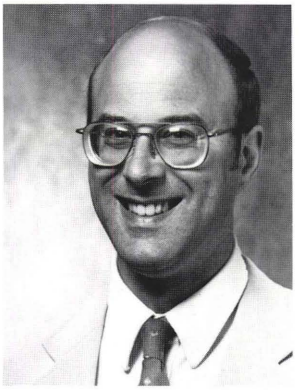

MICHAEL E. THOMAS received a B.E.E. from the University of Dayton and an M.S. and Ph.D. from Ohio State University. He joined APL in 1979 and has been working on electromagnetic propagation and optical properties of materials. In 1982, he was a postdoctoral fellow in the Department of Physics, Naval Postgraduate School. In 1988, Dr. Thomas became a part-time G.W.C. Whiting School of Engineering faculty member, teaching courses on optical propagation and lasers. Current research interests include experimental and theoretical modeling of atmospheric propagation in IR, DIAL lidar, optical and IR window materials, and the IR properties of high-pressure gases. He has published over fifty book and journal articles in these fields. Dr. Thomas is a senior member of IEEE and holds membership in the Optical Society of America, SPIE, and Tau Beta Pi.

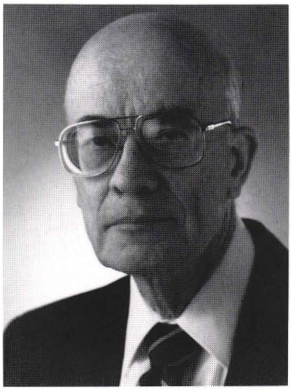

FRANK F. MARK studied physics at MIT and is a member of the Advanced Systems Group of APL's Aeronautics Department. His work is in the fields of fluid dynamics, biomedical research, optics, and advanced materials.